Journal of Solid State Chemistry 227 (2015) 25–29

Contents lists available at ScienceDirect

Journal of Solid State Chemistry

journal homepage: www.elsevier.com/locate/jssc

Structural and electronic properties of Li-ion battery cathode material MoF_3 from first-principles

A.Y. Li [a], S.Q. Wu [b], Y. Yang [c], Z.Z. Zhu [b,d,*]

[a] School of Opto-electronic and Communication Engineering, Xiamen University of Technology, Xiamen 361024, China
[b] Department of Physics and Institute of Theoretical Physics and Astrophysics, Xiamen University, Xiamen 361005, China
[c] State Key Lab for Physical Chemistry of Solid Surfaces, Xiamen University, Xiamen 361005, China
[d] Fujian Provincial Key Laboratory of Theoretical and Computational Chemistry, Xiamen University, Xiamen 361005, China

ARTICLE INFO

Article history:
Received 20 January 2015
Received in revised form
6 March 2015
Accepted 18 March 2015
Available online 27 March 2015

Keywords:
MoF_3
Electronic structures
Magnetism
First-principles

ABSTRACT

The transition metal fluorides have been extensively investigated recently as the electrode materials with high working voltage and large capacity. The structural, electronic and magnetic properties of MoF_3 are studied by the first-principles calculations within both the generalized gradient approximation (GGA) and GGA+U frameworks. Our results show that the antiferromagnetic configuration of MoF_3 is more stable than the ferromagnetic one, which is consistent with experimental results. The analysis of the electronic density of states shows that MoF_3 is a Mott–Hubbard insulator with a *d–d* type band gap, which is similar to the case of FeF_3. Moreover, small spin polarizations were found on the sites of fluorine ions, which accords with a fluorine-mediated superexchange mechanism for the Mo–Mo magnetic interaction.

1. Introduction

Lithium-ion batteries (LIBs) have undergone widely scientific research and shown successful commercial applications in a variety of portable electronic devices and electric vehicles [1,2]. At present, $LiCoO_2$ is utilized as a cathode in most of the commercial lithium ion batteries [3,4], however, the active reversible specific capacity of $LiCoO_2$ is below 150 mA h g^{-1} which cannot well meet the requirement of the power lithium ion battery. To satisfy the demand for the electric vehicles, much attention has been paid to the development of new systems, in particular to those with high energy density and discharge voltage which can store more energy at reduced weight [5–11]. In a way, the choice of cathode materials is very important. Good cathode material can accommodate a large amount of Li-ions, which can supply high capacity. Recently, as a special class of promising cathode materials, transition metal fluorides have attracted great interest due to high ionicity which can provide high operating voltage in Li-ion batteries [12–15]. Metal fluorides enable the highest specific capacity via the large multi-electron reversible redox conversion process through the following reaction scheme:

$$xLi^+ + xe^- + MoF_x \leftrightarrow xLiF + Mo$$

However, the highly ionic nature of M–F bond leads to an insulating character of MF with poor electronic conductivity and limits their discharge voltage. For example, the discharge capacity of FeF_3 (80 mA h g^{-1}) first reported by Arai et al. [16] is far below the theoretical $1e^-$ transfer reaction capacity of the Fe^{3+}/Fe^{2+} couple (237 mA h g^{-1}). Fortunately, electronic limitations are no longer an insurmountable issue in design of high-performance electrode material. Low conductivity can be improved through various materials processing approaches, including the use of carbon coatings, mechanical grinding, mixing [17], and low-temperature synthesis routes [14] to obtain tailored particles. Among transition metal fluorides, FeF_3, CuF_2 [18] are widely investigated, however, little has been done on MoF_3. As is well known, molybdenum is a multi-valence-electron element which could enable a six-electron reversible process resulting in specific high capacities. Therefore, element Mo has been very active in the field of lithium ion batteries. Molybdenum disulfide and molybdenum oxide are well-known lithium insertion compounds and have been much investigated [19,20]. Moreover, experiments [21] have shown that MoF_3 and FeF_3 have the same crystal structure and magnetic structure. The magnetic ground state of MoF_3 or FeF_3 is antiferromagnetism (AFM), in which each metal atom is antiferromagnetically coupled through the intervening fluorine atoms to each of its six nearest neighbors. Consequently, it is of great interest to explore and understand the intrinsic structural properties and electronic characteristics of

* Corresponding author at: Fujian Provincial Key Laboratory of Theoretical and Computational Chemistry, Xiamen University, Xiamen 361005, China. Tel.: +86 592 2182248; fax: +86 592 2189426.
E-mail address: zzhu@xmu.edu.cn (Z.Z. Zhu).

http://dx.doi.org/10.1016/j.jssc.2015.03.019
0022-4596/

the MoF_3 material. In this paper, we focus on the study of ground state properties of MoF_3, by analyzing the structural, magnetic, and electronic properties from first-principles calculations.

The present calculations have been performed by using the Vienna ab initio simulation package (VASP) [22,23], which is based on the density functional theory, the plane-wave basis, and the projector augmented wave (PAW) representation [24]. The exchange correlation potentials are approximated by the generalized gradient-corrected approximation (GGA) [25]. To address the on-site Coulomb interactions in the localized *d* electrons of Mo ions, the GGA+U method with an additional Hubbard-type U term [26] was employed. Here, an $U_{eff}=U-J=2$ eV is used in this paper. In the study of magnetism of MoO_2,Wang et al. [27] used a range of values for U_{eff} between 1 and −1 eV, citing weak correlations in Mo. Jain and Hautier [28] more accurately predicted the formation enthalpies of 49 ternary oxides by mixing GGA and GGA+U energies, they arrived at a value of $U_{eff}=3.5$ for Mo. Saitoh et al. [29] suggested a value of $U_{eff}=1.0$ for Mo based on a comparison of the computed band structure with valence-band photoemission spectra of single crystals of Sr_2FeMoO_6. We, therefore, take an average value of $U_{eff}=2.0$ eV. The wave functions were expanded in plane-wave basis up to a kinetic energy cutoff of 500 eV. Brillouin-zone integrations were performed by using special *k*-point sampling of the Monkhorst–Pack scheme [30] with a $4\times4\times2$ grid. The convergence of total energy with respect to the kinetic energy cutoff and the *k*-point sampling has been examined. The atomic geometry of MoF_3 was fully relaxed until the Hellmann–Feynman forces on all atoms were less than 0.01 eV $Å^{-1}$. The unit cell adopted for the present calculation contains 6 formula unit of MoF_3, which is 24 atom per unit cell (18 fluorine atoms and 6 Mo atoms).

Several experimental studies [21,31] have shown that MoF_3 has a bimolecular rhombohedral unit cell of space group $R\bar{3}c$. The hexagonal representation of the lattice, as shown in Fig. 1, is related to a collapsed ReO_3 perovskite structure. The Mo–F–Mo bond angle is deviated from the ideal 180° (experimental value of 141.02° [31]). MoF_3 also exhibits a layered structure and comprises corner-sharing $MoF_{6/2}$ octahedra. In Table 1, we have presented the calculated lattice parameters, the bond length of Mo–F, the bond angle of Mo–F–Mo and the spin magnetic moments of Mo and F ions in MoF_3. Both of the GGA and GGA+U calculations predict that the AFM configuration is more favorable. The differences of cohesive energies (per molecular formula) between antiferromagnetic and ferromagnetic configurations are 0.476 eV for GGA and 0.234 eV for GGA+U calculations, respectively. Their lattice parameters calculated within the GGA+U scheme are larger than those calculated within the GGA.

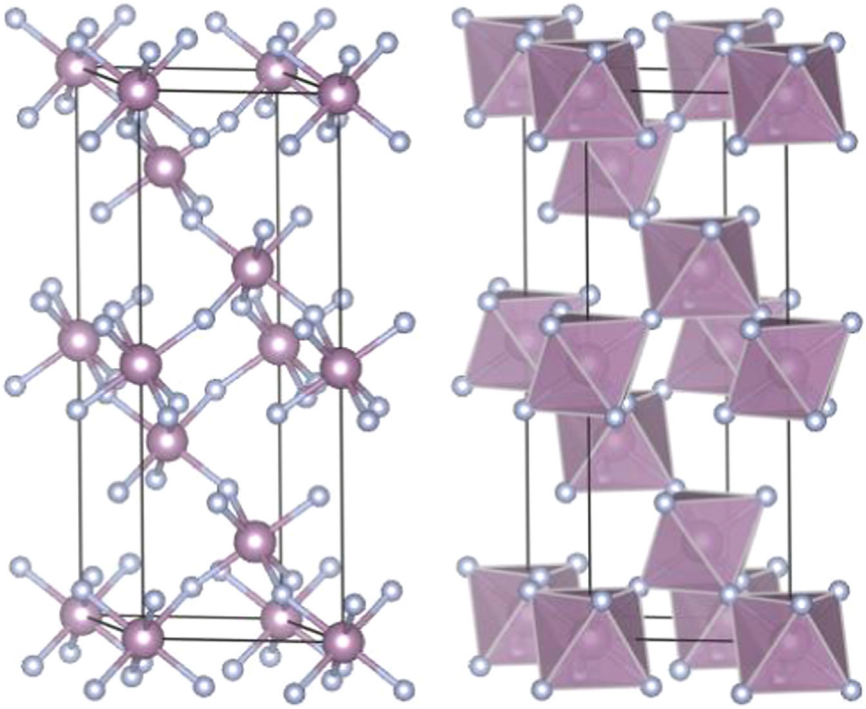

Fig. 1. The crystal structure of MoF_3 in the hexagonal structure. The Mo and F atoms are denoted by larger and smaller balls, respectively. Mo–F_6 octahedra are also shown in the right panel.

Table 1
The optimized lattice parameters, the cohesive energies E_c (in eV/molecular formula), the Mo–F bond lengths, the bond angles of Mo–F–Mo, and the magnetic moments of Mo and F ions of MoF_3 for the FM and AFM configurations calculated by both the GGA and GGA+U schemes, together with the experimental data [31].

Method	*a* (Å)	*c* (Å)	E_C (eV)	R_{Mo-F} (error) (Å)	∠Mo–F–Mo (°)	*m* (Mo) (μB)	*m* (F) (μB)
AFM [31]	5.213	14.41	–	2.04	141.02		
FM: GGA	5.276	14.492	152.098	2.07 (1.4%)	139.37	2.689	0.054
FM: GGA+U	5.410	14.782	145.350	2.08 (1.9%)	139.80	3.053	0.021
AFM: GGA	5.388	14.395	152.574	2.06 (0.9%)	145.10	2.513	0
AFM: GGA+U	5.386	14.557	145.584	2.08 (1.9%)	143.16	2.721	0

Experiments show that MoF_3 is an insulator, and its magnetic susceptibility is of temperature dependence which reveals the antiferromagnetic character of this compound [21]. These measurements also attribute a Néel temperature of 185 K to MoF_3. To gain further insight into the electronic structure of MoF_3, the total density of states (TDOS) in the antiferromagnetic configuration calculated by GGA+U scheme, together with the Mo-4*d* and F-2*p* partial density of states (PDOS), has been shown in Fig. 2. The TDOS of AFM-MoF_3 is shown to be divided into several regions. The peak around −3.5 eV is of mainly F-2*p* character. In the energy region below −4.8 eV, the TDOS shows significant contributions from both the Mo-4*d* and F-2*p* states. i.e., showing a strong hybridization of Mo-4*d* and F-2*p* atomic orbitals. A narrow band located at −0.5 to 0.0 eV are from the Mo-4*d* orbital. For the conduction bands (around 3 to 5 eV), the contributions are also almost fully from the Mo-4*d* orbital.

In order to comprehend the electronic properties of MoF_3 more clearly, the DOS for the ferromagnetic configuration is also calculated by both the GGA and GGA+U methods, and results are presented in Fig. 3 for comparison. Fig. 3 suggests that the electronic structures for both the AFM and FM configurations predicted by the GGA method are similar to those by the GGA+U scheme, in addition to the values of band gaps. The GGA calculations predicted a semiconductor character for MoF_3 with band gaps of 1.42 eV for AFM and 0.87 eV for FM, respectively. However, GGA+U calculations indicated that MoF_3 is an insulator with band gaps of 2.59 eV for AFM and 1.92 eV for FM configurations, respectively. Obviously, GGA+U calculations show better size of band gap for MoF_3. Because of the well-known band-gap problem in the density functional theory, the size of the band gap should be well underestimated by the GGA method. The wide energy gap of MoF_3 results in poor electronic conductivity which might likely restrict the application of MoF_3 as cathode materials. However, electronic conductivity limitation might be overcome through several materials processing approaches, including the use of carbon coating, mechanical grinding or mixing, and low-temperature synthesis routes to obtain tailored particles. From Fig. 3, it is also shown that the DOS peaks at valence-band maximum and conduction-band minimum for AFM states are much more localized than those of FM ones, from both the GGA and GGA+U calculations. Since the valence-conduction band gap is separated by Mo-*d* states, MoF_3 is then a Mott–Hubbard insulator like FeF_3 and FeF_2 [32,33], rather than a charge-transfer insulator.

To visualize the nature of the bond character, to explain the charge transfer and the bonding properties of MoF_3, the deformation charge density plot for the plane containing two F–Mo bonds of MoF_3 is shown in Fig. 4(a). The deformation charge density, $\Delta\rho(\vec{r})$, is defined as the difference between the total charge density in the solid and the superposition of independent atomic charge densities placed at the atomic sites of the same solid, i.e.,

$$\Delta\rho(\vec{r}) = \rho(\vec{r}) - \sum_{\mu} \rho_{\text{atom}}(\vec{r} - \vec{R}_{\mu})$$

where $\vec{R}_{\mu}$ are the atomic coordinates. Only the results from GGA+U approach in the AFM configuration is presented in Fig. 4(a), because GGA method presents similar maps for the deformation charge

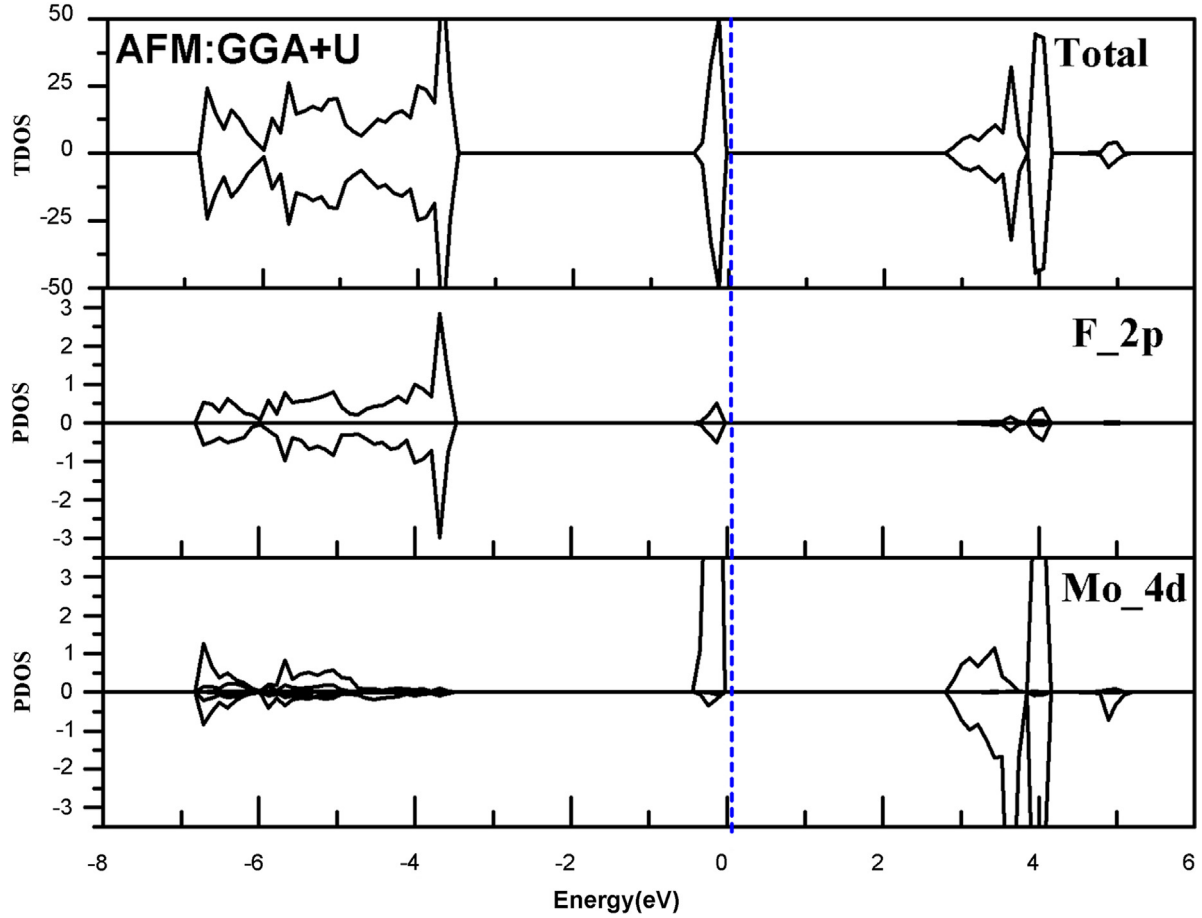

Fig. 2. The spin-polarized total density of states (TDOS) for MoF_3 and partial density of states (PDOS) for F-2*p* and Mo-4*d* orbitals predicted by GGA+U method for antiferromagnetic state of MoF_3. The valence-band maximum is shown by the vertical dot line. The unit of TDOS is states/eV unit cell.

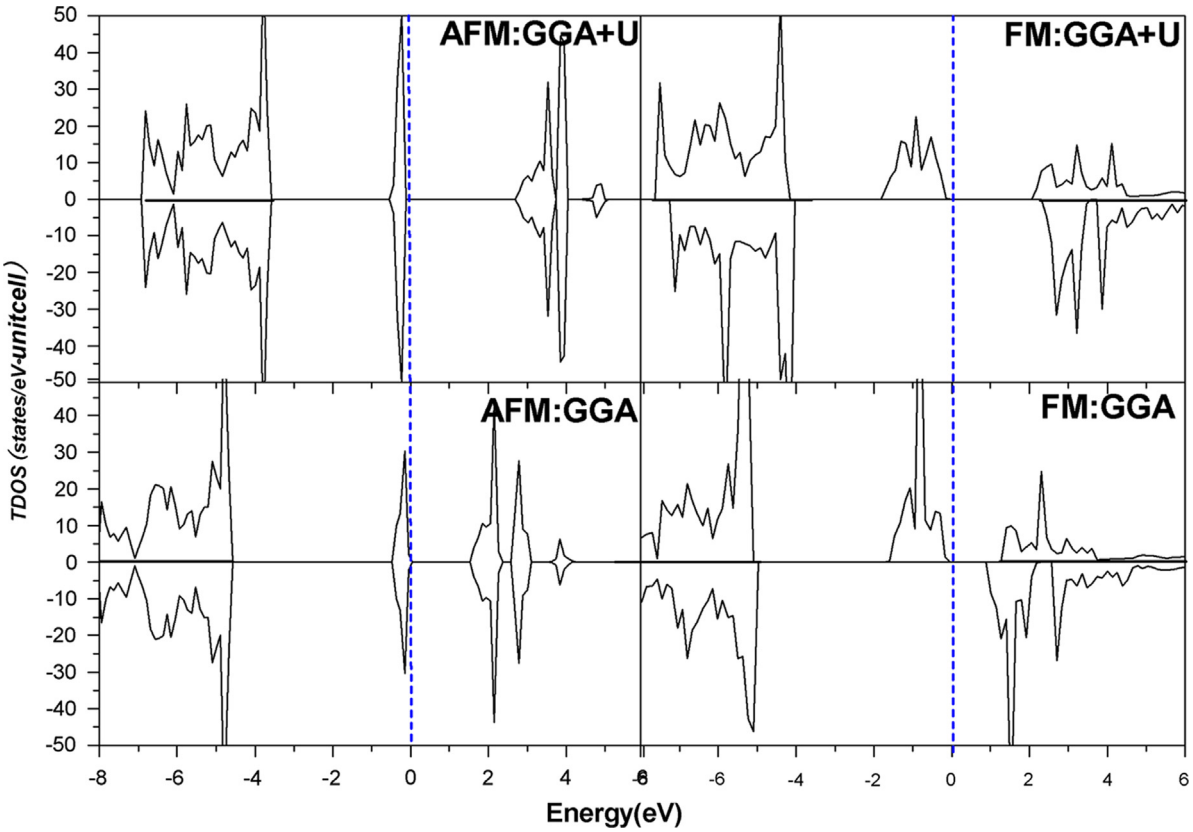

Fig. 3. The total density of states for the MoF_3 in the AFM and FM configurations calculated by both GGA+U and GGA schemes. The valence-band maximum is shown by the vertical dot line.

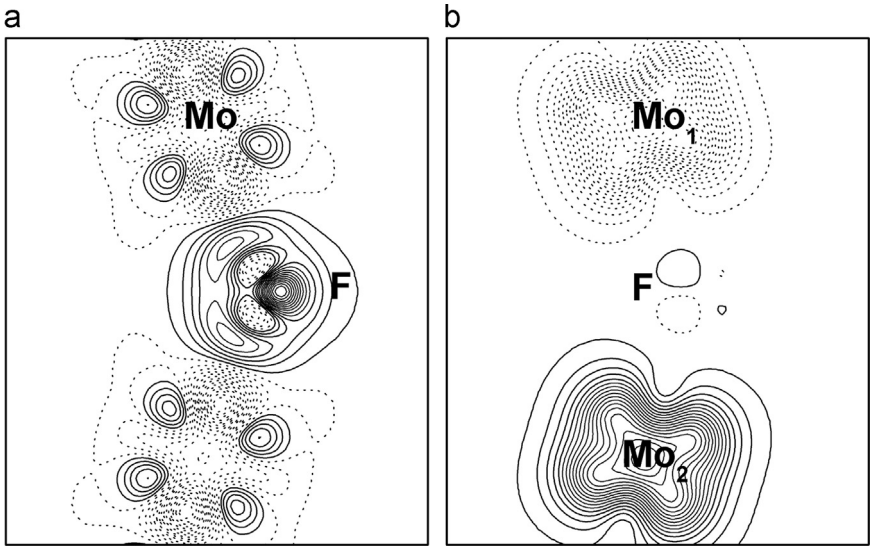

Fig. 4. Contour plots on the Mo–F–Mo plane of the (a) deformation charge density and (b) spin-density for MoF_3 in the AF configuration calculated with GGA+U scheme. Isodensity curves are separated by (a) 0.028 and (b) 0.061 e $Å^{-3}$. Solid and dot dash lines correspond to positive and negative values, respectively.

density. The bonding between Mo and F shows prominent ionic characteristics as well as some covalency, in line with the high electronegativity of the F atom. Charge polarizability and dipole-dipole interactions have been proved as the major influences on the stabilization of tilts of corner coupled rigid octahedrons.

To further understand the magnetic properties, the calculated spin charge density plots (i.e., the spin-up charge density minus the spin-down one) for the AFM configuration from the GGA+U calculations is given in Fig. 4(b). The magnetism of MoF_3 is mainly expressed by Mo, as expected. As shown in Fig. 4(b), there is a net excess of spin-down over spin-up electrons around the site of Mo_1, while the neighboring atoms of Mo_1, i.e., Mo_2, has a net spin-up electrons. The spin-up and spin-down electron distributions are almost identical, showing an AFM configuration in the ground state of MoF_3. Mo shows also remarkable high-spin magnetism. On the other hand, it is very interesting to remark that fluorine exhibits a small magnetism as well. On the sites of fluorine ions, a very small spin polarization is clearly visible in Fig. 4(b). Such spin polarizations on the sites of F ions are convincing evidence for the fluorine-mediated superexchange mechanism for the Mo–Mo

magnetic interaction. Similar effect of spin electron transfer and superexchange mechanism were discussed before in FeF_3 [32] and FeF_2 [33].

In summary, we have performed first-principles calculations based on the density functional theory within the GGA and GGA+U schemes to predict the structural properties and electronic structures of MoF_3 in both the ferromagnetic and antiferromagnetic states. Our results show that GGA+U approximation provided more reasonable predictions on the structural and electronic properties of MoF_3, in consideration of the strongly correlated 4*d*-electron orbitals of Mo atoms. By comparing cohesive energies in the AFM and FM configurations, the MoF_3 in AFM turns out to be more stable, consistent with experiments. The electronic structure calculations indicate that MoF_3 is an insulator with strong ionic character and a large band gap. Furthermore, analysis of the electronic density of states suggests that MoF_3 is a Mott–Hubbard insulator with a *d*–*d* type band gap. Moreover, small spin polarizations are found on the sites of F-ions, which is in agreement with a picture of fluorine-mediated superexchange mechanism for the Mo–Mo magnetic interaction.

Acknowledgments

This work is supported by the National Natural Science Foundation of China under Grant no. 21233004 and the Scientific Research Foundation of Fujian Provincial Education Department (Grant no. JK2011045).

References

[1] M. Armand, J.M. Tarascon, Nature 451 (2008) 652.
[2] J.M. Tarascon, M. Armand, Nature 414 (2001) 359.
[3] J. Li, R. Klöpsch, M.C. Stan, S. Nowak, M. Kunze, et al., J. Power Sources 196 (2011) 4821.
[4] C.Q. Zhu, C.H. Yang, W.D. Yang, C.Y. Hsieh, J. Alloys Compd. 496 (2010) 703.
[5] R.B. Araujo, R.H. Scheicher, J.S. de Almeida, A.F. da Silva, R. Ahuja, Solid State Commun. 173 (2013) 9.
[6] J.M. Wang, J.P. Hu, C.Y. Ouyang, S.Q. Shi, M.S. Lei, Solid State Commun. 151 (2011) 234.
[7] Y. Yamada, T. Doi, I. Tanaka, S. Okada, J. Yamaki, J. Power Sources 196 (2011) 4837.
[8] I. Bhaumik, S. Kumar, S. Ganesamoorthy, R. Bhatt, A.K. Karnal, B.N.R. Sekhar, Solid State Commun. 151 (2011) 1869.
[9] H. Kim, D.J. Kim, D.H. Seo, M.S. Yeom, K. Kang, D.K. Kim, Y. Jung, Chem. Mater. 24 (2012) 1205.
[10] H. Kim, R.A. Shakoor, C. Park, S.Y. Lim, J.S. Kim, K. Miyasaka, R. Kahraman, Y. Jung, J.W. Choi, Adv. Funct. Mater. 23 (2013) 1147.
[11] Y. Zheng, P. Zhang, S.Q. Wu, Y.H. Wen, Z.Z. Zhu, Y. Yang, J. Electrochem. Soc. 160 (2012) A927.
[12] M. Nishijima, I.D. Gocheva, S. Okada, T. Doi, J. Yamaki, T. Nishida, J. Power Sources 190 (2009) 558.
[13] P. Liao, B.L. MacDonald, R.A. Dunlap, J.R. Dahn, Chem. Mater. 20 (2008) 454.
[14] T. Li, L. Li, Y.L. Cao, X.P. Ai, H.X. Yang, J. Phys. Chem. C 114 (2010) 3190.
[15] F. Badway, F. Cosandey, N. Pereira, G.G. Amatucci, J. Electrochem. Soc. 150 (2003) A1318.
[16] H. Arai, S. Okada, Y. Sakurai, J. Yamaki, J. Power Source 68 (1997) 716.
[17] F. Badway, N. Pereira, F. Cosandey, G.G. Amatucci, J. Electrochem. Soc. 150 (9) (2003) A1209.
[18] A.N. Mansour, F. Badway, W.-S. Yoon, K.Y. Chung, G.G. Amatucci, J. Solid State Chem. 183 (2010) 3029.
[19] G.D. Du, Z.P. Guo, S.Q. Wang, R. Zeng, Z.X. Chen, H.K. Liu, Chem. Commun. 46 (2010) 1106.
[20] S.H. Lee, Y.H. Kim, R. Deshpande, A.C. Dillon, Adv. Mater. 20 (2008) 3627.
[21] M.K. Wilkinson, E.O. Wollan, H.R. Child, J.W. Cable, Phys. Rev. 121 (1961) 74.
[22] G. Kresse, J. Furthmüller, Phys. Rev. B 54 (1996) 11169.
[23] G. Kresse, J. Furthmüller, Comput. Mater. Sci. 6 (1996) 15.
[24] P. Blöchl, Phys. Rev. B 50 (1994) 17953.
[25] J.P. Perdew, J.A. Chevary, S.H. Vosko, K.A. Jackson, M.R. Pederson, D.J. Singh, C. Fiolhais, Phys. Rev. B 46 (1992) 6671.
[26] I.V. Solovyev, P.H. Dederichs, Phys. Rev. B 50 (1994) 16861.
[27] F.G. Wang, Z.Y. Pang, L. Liang, S.H. Han, Phys. Rev. B 81 (2010) 134407.
[28] A. Jain, G. Hautier, G. Ceder, Phys. Rev. B 84 (2011) 045115.
[29] T. Saitoh, M. Nakatake, A. Kakizaki, Phys. Rev. B 66 (2002) 035112.
[30] H.J. Monkhorst, J.D. Pack, Phys. Rev. B 13 (1976) 5188.
[31] F. Averdunk, R. Hoppe, J. Less-Common. Met. 161 (1990) 135.
[32] R.F. Li, S.Q. Wu, Y. Yang, Z.Z. Zhu, J. Phys. Chem. C 114 (2010) 16813.
[33] G. Valerio, M. Catti, R. Dovesi, R. Orlando, Phys. Rev. B 52 (1995) 2422.